Identifying vacancy complexes in compound semiconductors with positron annihilation spectroscopy: A case study of InN

Christian Rauch,[1,*] Ilja Makkonen,[2] and Filip Tuomisto[1]

[1]*Department of Applied Physics, Aalto University, P.O. Box 11100, FI-00076 Aalto, Espoo, Finland*

[2]*Helsinki Institute of Physics and Department of Applied Physics, Aalto University, P.O. Box 14100, FI-00076 Aalto, Espoo, Finland*

(Received 14 April 2011; published 2 September 2011)

We present a comprehensive study of vacancy and vacancy-impurity complexes in InN combining positron annihilation spectroscopy and *ab initio* calculations. Positron densities and annihilation characteristics of common vacancy-type defects are calculated using density functional theory, and the feasibility of their experimental detection and distinction with positron annihilation methods is discussed. The computational results are compared to positron lifetime and conventional as well as coincidence Doppler broadening measurements of several representative InN samples. The particular dominant vacancy-type positron traps are identified and their characteristic positron lifetimes, Doppler ratio curves, and line-shape parameters determined. We find that indium vacancies (V_{In}) and their complexes with nitrogen vacancies (V_{N}) or impurities act as efficient positron traps, inducing distinct changes in the annihilation parameters compared to the InN lattice. Neutral or positively charged V_{N} and pure V_{N} complexes, on the other hand, do not trap positrons. The predominantly introduced positron trap in irradiated InN is identified as the isolated V_{In}, while in as-grown InN layers V_{In} do not occur isolated but complexed with one or more V_{N}. The number of V_{N} per V_{In} in these complexes is found to increase from the near-surface region toward the layer-substrate interface.

DOI: 10.1103/PhysRevB.84.125201 PACS number(s): 61.72.jd, 78.70.Bj, 71.60.+z, 61.72.Yx

I. INTRODUCTION

InN is a significantly cation-anion mismatched semiconductor compound[1] with many interesting properties and promising applications in optoelectronics and high-speed electronics.[2] Intrinsic point defects have been accounted for multiple important mechanisms in the material.[3–7] Among them, isolated and complexed In vacancies (V_{In}) and N vacancies (V_{N}) are expected to be the dominant intrinsic acceptors and donors, respectively, according to latest density functional theory calculations.[8–12] Nevertheless, unambiguous experimental evidence on their nature and characteristics is still relatively scarce. This is due to limitations stemming from intrinsic properties of InN, as well as challenges related to the growth of high-quality material. Strong surface electron accumulation in polar samples[13] complicates the fabrication of Schottky contacts and therefore the application of standard electrical characterization methods such as deep level transient spectroscopy (DLTS) and capacitance voltage (C-V) profiling. Additionally, the high conductivities common for early as-grown InN layers, together with the unavailability of bulk material, strongly limit the use of electron paramagnetic resonance (EPR)-based techniques.

Positron annihilation spectroscopy is a powerful method for the investigation of vacancy-type defects in semiconductors[14] and is largely not affected by the above-mentioned challenges. Positrons can get trapped and annihilate at neutral and negatively charged open volume sites in the crystal lattice due to a locally reduced Coulomb repulsion. This increases the positron lifetime and narrows the momentum distribution of annihilating electron-positron (e-p) pairs, both of which can be measured by recording the emitted annihilation γ radiation.

While direct experimental evidence on the behavior of V_{N} has been very limited, previous positron annihilation results show that V_{In} related defects are incorporated in concentrations of $\sim 10^{16}$–10^{17} cm^{-3} during growth of both molecular beam epitaxy (MBE)[15–17] and metalorganic chemical vapor deposition (MOCVD)[18] InN. Although V_{In} related defect concentrations in thick layers of high-quality as-grown material are found to be low, in the 10^{16} cm^{-3} range,[17] the experimentally observed concentrations are still by orders of magnitude higher than what could be expected based on first-principles calculations.[8,12] A strong influence of the layer thickness on the vacancy concentrations has been found,[15] together with a commonly observed increase and qualitative change of the vacancy signal when approaching the layer-substrate interface.[7,15,18,19] Growth parameters such as polarity[7] and stoichiometry[17,18] seem to have only a minor impact. This suggests that the vacancy formation in InN is not dominated by thermal equilibrium processes but rather controlled by mechanisms such as local strain, the vicinity to other point and extended defects, and/or limited surface diffusion during growth.[17] Nevertheless, to the best of our knowledge, no direct correlation between dislocation densities and vacancy formation has been found so far.[17,20] In good agreement with the behavior of negatively charged defects below the branch point energy,[1,21] n-type doping of InN by either Si (Refs. 19 and 22) or high-energy particle irradiation[6] leads to an increasing incorporation of V_{In} related defects, while Mg-doped samples (with lowered Fermi-level positions) show only low concentrations.[23]

Unfortunately, the exact chemical identity of the vacancy defects detected in previous studies has remained largely unknown. Recent attempts, however, have shown that these limitations could in principle be overcome by careful modeling of positron annihilation parameters using *ab initio* calculations.[23–25] Despite this, to the best of our knowledge, a comprehensive theoretical study of positron annihilation in InN is still missing.

In the following, we present an extensive identification of common vacancy and vacancy-impurity complexes in InN by

combining positron annihilation spectroscopy and *ab initio* calculations. The employed computational and experimental methods are presented in Sec. II. Calculated positron lifetimes and momentum distributions of annihilating e-p pairs are shown in Sec. III for a variety of vacancies and vacancy complexes in InN. In Sec. IV these are compared to experimental data from positron lifetime and Doppler broadening measurements, and the dominant vacancy defects in positron annihilation measurements of different as-grown, doped, and irradiated InN samples are identified. A critical discussion of the results is presented in Sec. IV D and possible implications are outlined.

II. METHODS

A. Experiment

Positron annihilation measurements are performed using a variable-energy (0.5–38 keV) slow positron beam. The Doppler broadening of the e-p annihilation radiation is recorded with two Ge detectors with a combined Gaussian resolution function of 1.24 keV (0.66 a.u.) and 0.995 MeV (0.53 a.u.) full width at half maximum (FWHM) at 0.511 MeV in the conventional and coincidence Doppler setup,[26,27] respectively. In the latter configuration, both annihilation photons are detected simultaneously and only counted if energy conservation is fulfilled ($E_{\mathrm{tot}} = 1.022$ MeV). This significantly improves the peak-to-background ratio up to 10^6 and sharpens the detector resolution. To assure statistical reliability, spectra of $\sim 1 \times 10^6$ and 3×10^7 counts are accumulated for each measurement point in the conventional and coincidence setup, respectively.

In the conventional Doppler mode the annihilation peak is analyzed using the common integrated line-shape parameters[14] which represent the annihilation fractions in the low (S) and high (W) momentum parts of the spectrum. Integration windows of $|p_L(S)| < 0.4$ a.u. ($\Delta E_\gamma < 0.75$ keV) and 1.5 a.u. $< |p_L(W)| < 3.9$ a.u. (2.9 keV $< \Delta E_\gamma <$ 7.3 keV) are chosen for the S and W parameters, respectively. In positron annihilation experiments the time-integrated annihilation parameter P_{exp} (e.g., average positron lifetime, annihilation line shape, S and W parameters) constitutes a weighted sum of the characteristic values of the present positron traps P_i and the crystal lattice P_b,

$$P_{\mathrm{exp}} = \eta_b P_b + \Sigma_{i=1}^{n} \eta_i P_i, \tag{1}$$

with η_b and η_i being the positron annihilation fractions of the lattice and the ith defect, respectively.

The characteristic defect parameter P_i of a certain positron trap hence can be extrapolated from the recorded experimental signal P_{exp}, if the bulk parameter and the positron annihilation fractions are known. The latter can be determined by decomposition of the positron lifetime spectrum into its n exponential decay components,[14] or by a complementary measurement of another time-integrated annihilation parameter whose set of characteristic parameters is well known. The bulk parameter is usually determined by measurement of a reference sample in which no trapping to vacancy defects can be observed (confirmed by positron lifetime measurements).

B. Computation

Our computational scheme[25] is based on the zero-positron-density limit of the two-component density functional theory.[28] Valence electron densities are calculated self-consistently using the local density approximation (LDA) and projector augmented-wave method (PAW)[29] implemented in the VASP code.[30] All electronic structure calculations are performed using a 96-atom InN wurtzite supercell. Ionic positions are relaxed with a convergence criterium of 0.01 eV/Å for forces. Indium $4d$ electrons are included as valence electrons and an energy cutoff of 400 eV is chosen. The Brillouin zone is sampled with a 3^3 Monkhorst-Pack $\mathbf{k}$-point mesh.

After deriving the electron densities in the lattice, the positron densities are solved independently in the calculated Coulomb potential due to electrons and nuclei and the e-p correlation potential. This is the so-called "conventional scheme", in which the positron does not affect the average electron density, and further, the e-p correlation potential is approximated in the zero-positron-density limit. This is only exact for the case of a completely delocalized positron in the crystal lattice (bulk), but is also justified for finite positron densities localized at a defect site when considering the positron and its screening cloud of electrons as a neutral quasiparticle which does not affect the surrounding average electron density. The LDA[28] in the state-dependent scheme[27] is used for the description of many-body effects in the calculation of positron annihilation rates and the momentum distributions of annihilating e-p pairs. In this approximation, the momentum density $\rho(\mathbf{p})$ of annihilating e-p pairs is expressed as

$$\rho(\mathbf{p}) = \pi r_e^2 c \sum_j \gamma_j \left| \int d\mathbf{r}\, e^{-i\mathbf{p}\cdot\mathbf{r}} \psi_+(\mathbf{r}) \psi_j(\mathbf{r}) \right|^2, \tag{2}$$

where r_e is the classical electron radius, c is the speed of light, and $\psi_+(\mathbf{r})$, $\psi_j(\mathbf{r})$ are the positron and electron wave functions, respectively. The summation is performed over all occupied electron states and γ_j is the position-independent electron-state-dependent enhancement factor[27] which takes into account the increase in annihilations due to the screening electron density around the positron.

In order to be able to compare the calculated three-dimensional (3D) momentum density to one-dimensional (1D) experimental spectra, we integrate the calculated spectra over the wurtzite m plane. To account for the experimental detector resolution, the calculated momentum distributions are additionally convoluted with a Gaussian resolution function of 0.53 and 0.66 a.u. FWHM for the comparison with coincidence and conventional Doppler spectra, respectively. The line-shape parameters S and W are calculated from the spectra convoluted with 0.66 a.u. FWHM using the above momentum windows. The positron lifetime τ is determined as the inverse of the annihilation rate λ, which is given as

$$\lambda = \frac{1}{\tau} = \pi r_e^2 c \int d\mathbf{r}\, n_+(\mathbf{r}) n_-(\mathbf{r}) \gamma(n_-(\mathbf{r})), \tag{3}$$

with $\gamma(n_-(\mathbf{r}))$ the enhancement factor[27] in the LDA.

In our calculations we made two further simplifications, i.e., all defects are considered in the neutral charge state and forces due to localized positrons are neglected. Adding negative (positive) charge is expected to lead to an additional inward

(outward) relaxation,[11] while the Coulomb force of localized positrons is directed outward.[25] The exact charge state of defect complexes is often unknown in experiments, hence it is not safe to be assumed without further proof. On the other hand, only considering the positron-induced forces[31] leads to an overestimation of the outward relaxation. Nevertheless, careful testing showed that the effects of additional charge and localized positrons on the annihilation characteristics can be neglected compared to changes between different defects. Also, trends in the calculated spectra are valid irrespective of which approximation is used.

III. COMPUTATIONAL RESULTS

The optimized lattice constants for wurtzite InN are calculated as $a = 3.510$ Å, $c = 1.610$ Å, and $u = 0.379$, in good agreement with literature.[11,32] The positron density in the InN lattice is fully delocalized [see Fig. 1(a)], and a positron lifetime of 157 ps is determined.

The difference compared to the experimentally determined lifetime value[15] of ∼180 ps stems from using the LDA enhancement factor. The choice of the LDA is motivated by our focus on the calculation of momentum distributions.[25] In this approximation, good agreement with experiments is achieved[25] for positron lifetime differences, $\Delta\tau = \tau_{\text{defect}} - \tau_{\text{bulk}}$, rather than absolute values. When analyzing computational positron lifetimes, it should be noted that calculated values are sensitive to the size of the relaxed open volume (i.e., overlap of positron and electron density), and small differences in relaxation of a few percent can lead to lifetime differences of a few ps.

The modeled momentum distribution of annihilating e-p pairs in the InN lattice is displayed in Fig. 2. The annihilation spectrum is symmetrical and hence is folded at its center at 0 a.u. (511 keV). In the low momentum part of the spectrum annihilations with In $5p$ and N $2p$ valence electrons dominate while contributions from tighter bound core electrons (In $4d$ and N $2s$) become more important in the higher momentum part of the spectrum.

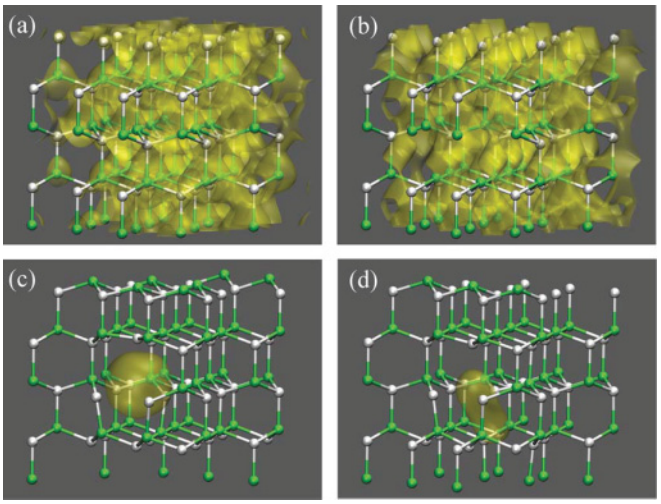

FIG. 1. (Color online) Isosurface plot of the calculated positron density (transparent sphere) in the relaxed lattice structure of the (a) InN lattice and (b) $4V_N$, (c) V_{In}, and (d) $2V_{In}$ defects. Light gray (silver) and dark gray (green) balls indicate N and In ions, respectively.

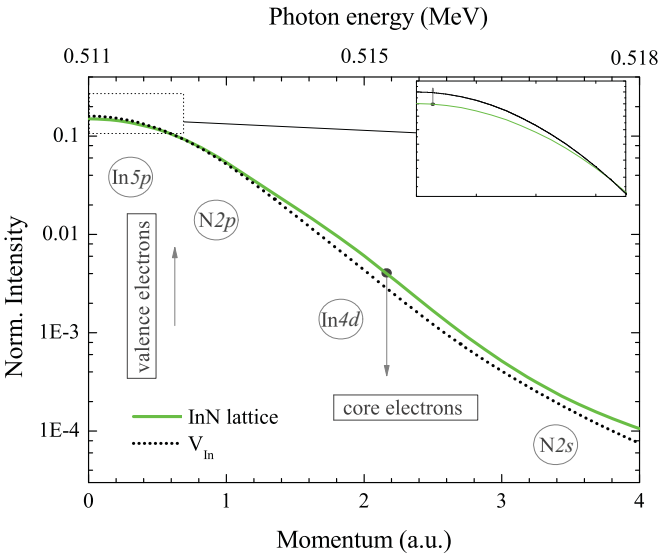

FIG. 2. (Color online) Calculated momentum density of annihilating e-p pairs in the delocalized state of the InN lattice and trapped at the V_{In}, respectively. Trends in the spectra are indicated with respect to the InN lattice.

A. Isolated In vacancy

The relaxed defect geometry of the V_{In} is shown in Fig. 1(c) together with the calculated positron density in the lattice. An outward relaxation of the neighboring N ions from their initial positions is observed in good agreement with Duan *et al.*[11] The positron density shows a strong localization at the defect site, which means that V_{In} act as efficient positron traps in InN. The calculated positron lifetime difference to the InN lattice is 85 ps, which is in good agreement with the ∼80 ps observed in experiments.[15,19] Results obtained with the atomic superposition (ATSUP) method[33] show for positrons trapped at the V_{In} increased annihilations with loosely bound valence electrons (In $5p$ and N $2p$), while annihilations with tighter bound core electrons (most importantly, In $4d$) decrease significantly. This leads to an overall narrowing of the annihilation peak compared to the InN lattice (see Fig. 2).

For a more detailed analysis of the momentum spectrum we examine its so-called ratio curve in Fig. 3(a), in which the calculated momentum distribution is displayed divided by the spectrum for the defect-free InN lattice to accentuate the defect-induced changes. The ratio curve for the V_{In} exhibits a distinct line shape with a maximum of ∼1.08 at the peak center region (0 a.u.). For momenta above 0.6 a.u. the spectrum drops below 1 and an articulate shoulder is visible at 1.2 a.u., which has been determined by ATSUP calculations to stem from annihilations with N $2p$ electrons. At ∼3.3 a.u. a second broad peak appears with an intensity of ∼0.8 relative to the InN lattice.

The characteristic relative line-shape parameters (for the conventional detector resolution of 0.66 a.u.) of the V_{In} momentum distribution spectrum are calculated as 1.057 and

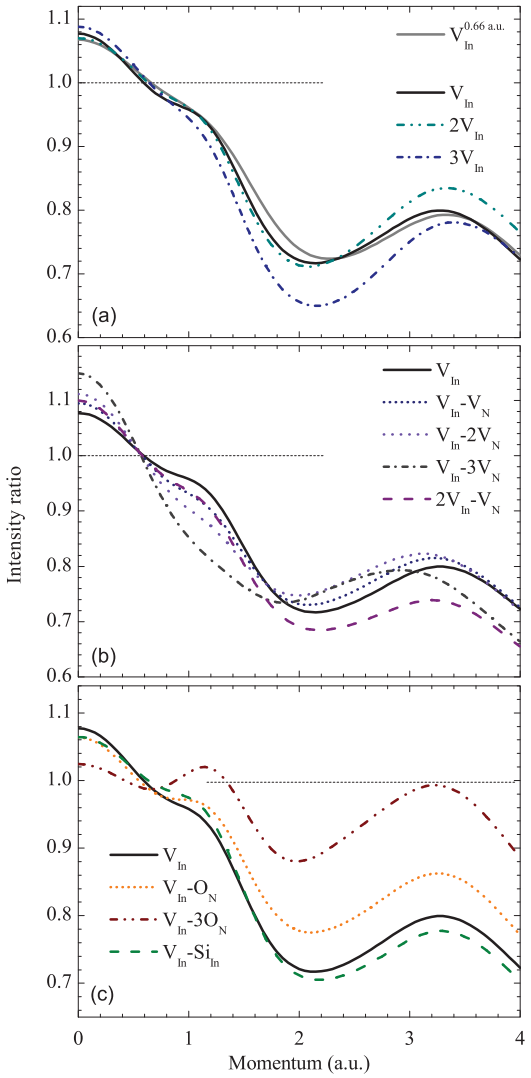

FIG. 3. (Color online) Ratio curves of the calculated momentum densities of annihilating e-p pairs in selected vacancy complexes in InN. All spectra are convoluted with a Gaussian of 0.53 a.u. FWHM (except $V_{In}^{0.66\ a.u.}$, FWHM = 0.66 a.u.) and divided by the momentum density spectrum of the InN lattice.

0.78 for S and W, respectively. Figure 4 shows the calculated values plotted in a SW plot.

B. In vacancy complexes

Recent DFT results[11] suggest that V_{In} would form complexes with each other and predict a significant decrease in formation energies when going from a single V_{In} to $2V_{In}$ and $3V_{In}$ complexes. Motivated by these results we calculate the momentum densities and positron lifetimes of the $2V_{In}$ and $3V_{In}$ in their most favorable configurations.[11] In the $2V_{In}$ pair the two vacancies are located out of plane (with respect to the c plane) on next-nearest-neighbor positions, and for the $3V_{In}$ complex an additional vacancy is added in the c plane sharing the same N atom. As expected, both $2V_{In}$ and $3V_{In}$ complexes show localized positron densities. Although the V_{In} are only situated on next-nearest-neighbor sites, their open volumes

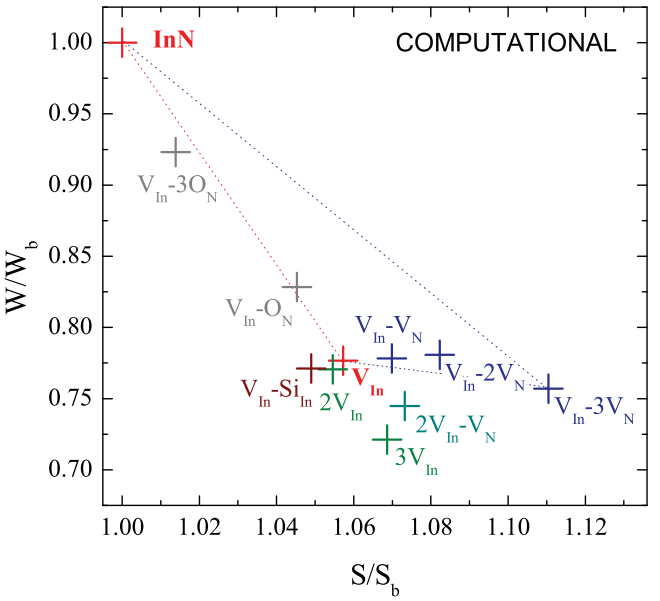

FIG. 4. (Color online) SW plot of conventional line-shape parameters S and W for the calculated momentum distributions of annihilating e-p pairs trapped at different vacancy-type defects in InN.

are connected, showing, e.g., a handlebar like structure for the positron density at the $2V_{In}$ pair [see Fig. 1(d)].

Positron annihilation characteristics of the $2V_{In}$ defect are very similar to the isolated V_{In}. The calculated positron lifetime is equal and the line-shape parameters are very close to the isolated case, with $\Delta\tau = 85$ ps, $S = 1.055$, and $W = 0.77$ (see Fig. 4). In the ratio curve in Fig. 3(a), a slight increase of the peak at 3.3 a.u. is visible but the absolute intensity at these momentum values is already reduced by $\sim 10^3$ compared to the peak maximum (see Fig. 2) and discrimination (in experiments) is hence considerably complicated.

For the $3V_{In}$ complex we calculate an increase in the positron lifetime of $\sim$10 ps compared to the isolated V_{In} ($\Delta\tau =$ 94 ps). Additionally, the ratio curve changes significantly with an increased peak maximum and a more pronounced drop at 2.1 a.u. This is also visible in the change of the line-shape parameters to $S = 1.069$ and $W = 0.72$. Nevertheless, further analysis shows that the relative line shapes of the $3V_{In}$ and V_{In} are very similar and the spectrum of the V_{In} can be nearly reproduced from the $3V_{In}$ spectrum by assuming a positron annihilation fraction of $\eta \approx 0.8$ [see Eq. (1)]. This is also visible in the SW plot (Fig. 4) in which the characteristic point of the $3V_{In}$ falls on an extension of the line connecting the InN lattice point and the V_{In}. For measurement points lying between the V_{In} and the InN lattice, the $3V_{In}$ and V_{In} can therefore only be distinguished with precise knowledge of the positron annihilation fraction. This is in practice limited by the achievable accuracy in the separation of lifetime components in positron lifetime measurements.

C. N vacancy complexes

For most of the Fermi-level regions, V_N in InN are supposed to be donors in the 3+ charge state[8] (hence repelling positrons) and possess a substantially smaller open volume compared to

the V_{In}, due to the large size difference between In and N atoms. Both suggest strongly that isolated V_N cannot act as positron traps in InN. Nevertheless, this may not account for larger complexes of several V_N which possess a positive binding energy (compared to isolated V_N) according to recent first-principles calculations.[9] The increased open volume in these defects could in principle promote a localization of the positron density. Additionally, the V_N complexes are assumed to adapt negative charge states for elevated Fermi-level positions which additionally support trapping.

To assess whether V_N or its complexes could act as positron traps in InN, we calculated the electron and positron densities for the isolated V_N and V_N complexes of up to four N vacancies in the neutral charge state. The defect structure and positron density for the $4V_N$ complex are shown in Fig. 1(b), exemplarily. We find that the positron density for all calculated V_N complexes is clearly delocalized and no bound positron state exists at V_N or V_N complexes. Hence, isolated V_N and pure V_N clusters (in the neutral charge state) cannot be detected using positron annihilation spectroscopy. For the case of negatively charged V_N complexes, the formation of weakly localized hydrogenic positron states around the defects is expected, which possess very similar annihilation characteristics to the defect-free lattice but might be detectable through their specific temperature behavior.[14]

D. Mixed In and N vacancy complexes

Apart from pure V_{In} and V_N complexes, a positive binding energy is predicted between isolated V_{In} and V_N, which should promote the formation of divacancies (V_{In}-V_N) and larger mixed vacancy complexes in the material.[11] We calculate the positron densities and positron annihilation characteristics for the relaxed lattice structures of a variety of mixed vacancy complexes in InN, namely, V_{In}-V_N, V_{In}-$2V_N$, $2V_{In}$-V_N, and V_{In}-$3V_N$. As expected, the increased open volume leads in all structures to a clear localization of the positron density at the defect site. The calculated positron lifetimes are close to the V_{In} lifetime for the V_{In}-V_N and V_{In}-$2V_N$, with $\Delta\tau = 86$ and 88 ps, but increase to 99 and 109 ps for the V_{In}-$3V_N$ and $2V_{In}$-V_N, respectively. Figure 3(b) shows the ratio curves of the computed momentum distributions. A systematic trend compared to the isolated V_{In} is visible in the spectra when adding an increasing amount of V_N around a single V_{In}. A strong increase of the zero momentum maximum to over 1.15 for the V_{In}-$3V_N$ is visible, which is related to the increase in open volume. At the same time, the intensity of the shoulder at 1.2 a.u. decreases with an increasing number of V_N until it entirely disappears for the V_{In}-$3V_N$. The ratio curve of the $2V_{In}$-V_N is close to the V_{In}-V_N for lower momentum values but starts to deviate at around 1.4 a.u. with lower intensities at higher momenta, due to reduced annihilation with In $4d$ electrons.

The characteristic line-shape parameters of the calculated complexes develop accordingly and show a clear deviation from the InN-V_{In} line in Fig. 4, which is already visible for the divacancy and intensifies with an increasing number of V_N. S and W values for the V_{In}-V_N, $2V_{In}$-V_N, V_{In}-$2V_N$, and V_{In}-$3V_N$ are determined as 1.070 and 0.78, 1.082 and 0.78, 1.073 and 0.75, and 1.115 and 0.76, respectively.

E. Vacancy-impurity complexes

III-vacancy donor-impurity complexes are well established in III-nitrides. In GaN, a binding energy of 1.6 eV has been determined[34] between O_N and V_{Ga}. The binding energy between between V_{Ga} and Si_{Ga} is considerably smaller (V_{Ga} and Si_{Ga} are only next-nearest neighbors) but still positive.[35] Recent *ab initio* calculations[10] predict also in InN a reduction of the defect formation energy for V_{In}-O_N complexes compared to the isolated case, and even stronger for the case of V_{In}-$3O_N$.

Hence, we take a look at the relaxed defect structures and positron densities for the V_{In}-O_N, V_{In}-$3O_N$ and V_{In}-Si_{In}. For all complexes the positron density is localized at the defect site. The calculated positron lifetimes to the InN lattice are again very close to the isolated V_{In} case with 85, 86, and 88 ps for the V_{In}-Si_{In}, V_{In}-O_N and the V_{In}-$3O_N$, respectively. In the ratio curves of the momentum densities shown in Fig. 3(c), the peak maximum decreases with increasing number of O ions, while the intensity in the spectral range above 0.9 a.u. increases including the shoulder at 1.2 a.u. and the peak at 3.4 a.u. The form of the V_{In}-O_N ratio curve resembles the case of V_{In} trapping with a reduced annihilation fraction of $\eta \approx 0.8$. This can also be seen in the *SW* plot (Fig. 4), where the characteristic points for all calculated vacancy impurity complexes roughly fall on the InN-V_{In} line, meaning that their line-shape parameters could be reproduced from the V_{In} values assuming incomplete annihilation fractions. The spectrum of the V_{In}-Si_{In} is very close the V_{In} and hence hardly distinguishable in experiments. The case is different for the ratio curve of the V_{In}-$3O_N$ which possesses distinct features with the shoulders at 1.2 and 3.6 a.u., respectively, which should be measurable in coincidence Doppler measurements. The corresponding line-shape S (W) parameters of the calculated vacancy-impurity complexes are 1.045 (0.83), 1.014 (0.92), and 1.049 (0.77) for the V_{In}-O_N, V_{In}-$3O_N$, and V_{In}-Si_{In}, respectively.

F. Summary and discussion

Our calculations can be summarized with the following conclusions. Isolated V_N and pure V_N complexes in the neutral or positive charge state do not localize the positron density and hence cannot be detected with positron annihilation spectroscopy. When negatively charged, they might act as shallow traps[14] for positrons. Isolated V_{In} are efficient positron traps in InN with annihilation characteristics (positron lifetime, ratio curve, line-shape parameters) which are clearly distinguishable from the InN lattice values. This is the case for all calculated defect complexes which include at least one V_{In}. Apart from the $2V_{In}$-V_N and V_{In}-$3V_N$ complexes, their calculated positron lifetime values are very similar with lifetime differences from 85 to 95 ps compared to the InN lattice value. Due to the experimental accuracy, their distinction based on characteristic defect lifetimes is in practice not feasible. The case is different for $2V_{In}$-V_N and V_{In}-$3V_N$ complexes, where lifetimes are higher, with 109 and 99 ps differences to the InN lattice, respectively.

A distinction between the isolated V_{In} and the calculated complexes can be achieved when considering their momentum distributions. For the characteristic line-shape parameters of mixed V_{In}-nV_N complexes, a clear deviation from the InN-V_{In} line is found in Fig. 4, with a strong increase of the S parameter

with a nearly constant W parameter for an increasing number of V_N around the V_{In}. Its origin is revealed in the corresponding ratio curves as a growing peak maximum and a nearly constant area for momenta between 1.5 and 3 a.u., where the dominant contributions to the S and W parameter, respectively, stem from. The most distinct feature of these V_{In}-$n V_N$ complexes is identified in the disappearing shoulder at 1.2 a.u.

The characteristic points of the calculated vacancy-impurity and pure V_{In} complexes do not show such a deviation but fall on (an extension of) the InN-V_{In} line. An accurate determination of the annihilation fractions would be necessary for an unambiguous identification of the $3V_{In}$ complex. The V_{In}-$3O_N$ complex exhibits some unique features in its ratio curve, but V_{In}-Si_{In} and $2V_{In}$ are hardly distinguishable from the isolated V_{In}.

IV. EXPERIMENTAL SPECTRA AND DEFECT IDENTIFICATION

In order to identify the dominant positron traps in common InN material we investigate a variety of as-grown and irradiated layers that were grown by different growth methods. An overview of a representative selection of measured samples is given in Table I. Sample I is MBE-grown material[6] which has been irradiated with 2-MeV He ions to a fluence of 8.9×10^{15} cm^{-2}, samples II and III are as-grown Si-doped[36] and undoped[37] InN layers deposited by MBE and MOCVD, respectively. Details on the growth and characteristics of the samples can be found elsewhere.[6,7,18,19,36,37] Samples I and II show a strong change in the Doppler broadening signal when approaching the interface, which is a common feature in several previously investigated InN samples.[7,15,18,19] Therefore, the interface region is investigated separately in these two samples (see Sec. IV C).

Conventional Doppler broadening (Fig. 5) as well as coincidence Doppler (Fig. 6) spectra are recorded for all samples. The recorded momentum distributions for samples I and II are extrapolated to saturation trapping, using annihilation fractions determined from previously recorded positron lifetime measurements. An extensive description of the positron lifetime data is published elsewhere.[7,19] All experimental momentum distributions are shown as ratio curves divided by the spectrum of a suitable reference for the InN lattice. The reference sample has been carefully analyzed using positron lifetime spectroscopy and no positron annihilation in trapped states at vacancy defects is observed.[38] All samples are measured perpendicular to the c axis.

TABLE I. Studied samples and experimentally determined line-shape parameters of the respective dominant positron trap. All parameters are extrapolated to saturation trapping and divided by the reference values measured in the InN lattice.

		Layer		Interface	
ID	Sample	S/S_{ref}	W/W_{ref}	S/S_{ref}	W/W_{ref}
I	MBE, irr.	1.042	0.80	1.083	0.78
II	MBE, Si-doped	1.051	0.83	1.077	0.81
III	MOCVD	1.052	0.81		

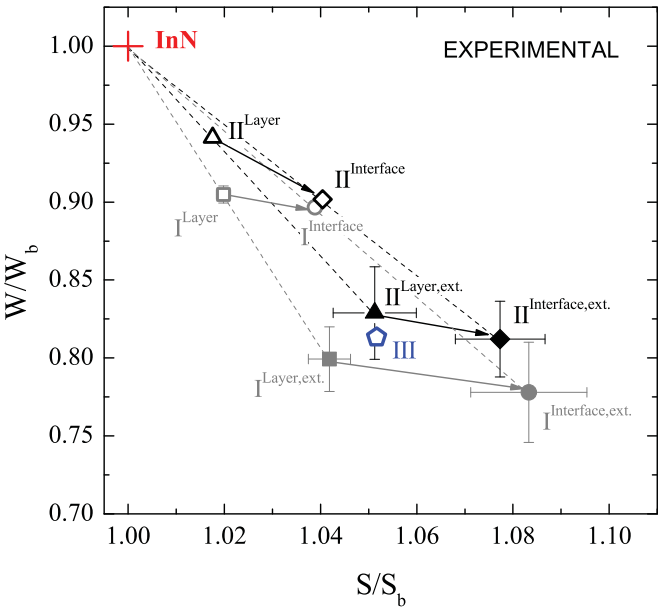

FIG. 5. (Color online) As-measured (open symbols) and extrapolated (closed symbols) line-shape parameters from conventional Doppler broadening measurements of different samples (see text for as-measured, and Table I for extrapolated values). Extrapolated points have been calculated using trapping fractions determined in positron lifetime measurements. For samples I and II, line-shape parameters for the near-surface ("layer") and near-interface region are given separately.

A. Irradiation-induced defects

Positron lifetime measurements[7] of the layer region of sample I show one dominant positron trap with a characteristic lifetime of 260 ps, and an annihilation fraction of $\eta = 0.47$ is determined for the trap. The recorded line-shape parameters ($S = 1.020$, $W = 0.90$) from conventional Doppler broadening measurements are extrapolated accordingly and displayed in Fig. 5. Characteristic line-shape parameters of $S = 1.042$ and $W = 0.80$ are evaluated for the dominant defect in this region.

The extrapolated ratio curve of sample I is shown in Fig. 6(a). When comparing the experimentally determined defect ratio curve to the calculated momentum distributions in Sec. II B we find good agreement with the spectrum of the isolated V_{In} for most of the spectral range. In the central region of the peak slightly higher intensities are found in the calculated spectrum compared to the experimental one. This region is mostly sensitive to the size of the open volume of the positron trap, with higher intensities for larger volumes. The calculated $2V_{In}$ and V_{In}-O_N complexes possess an overall rather similar shape of the ratio curve, and based on this also have to be considered as possible sources of the defect signal. Nevertheless, the available lifetime data do not support the reduced annihilation fraction which would be required for an identification of the experimental spectrum with the V_{In}-O_N. Although the differences between the V_{In} and $2V_{In}$ complexes are more subtle and hence the $2V_{In}$ cannot be ruled out as contributing to the signal, the ratio curve of the V_{In} gives the best overall approximation of the experimental spectrum.

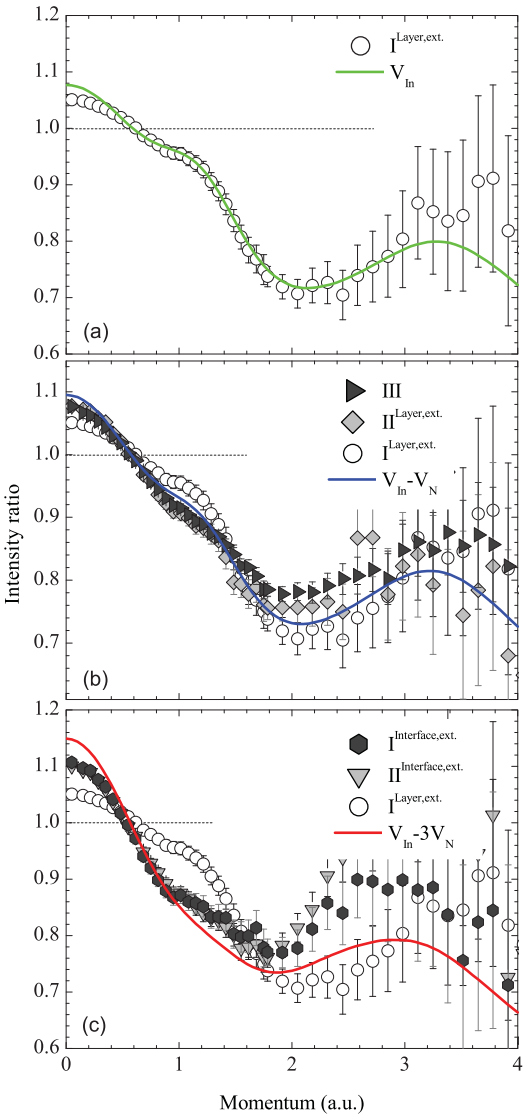

FIG. 6. (Color online) Experimental coincidence Doppler spectra of the investigated samples in the layer (a), (b) and interface (c) region. The data has been divided by a suitable reference spectrum for the InN lattice. Computational ratio curves are shown for comparison.

Therefore, we identify the positron trap created in irradiated InN with the isolated V_{In}.

B. Defects in as-grown samples

The experimentally determined S and W parameters from conventional Doppler broadening measurements for the as-grown samples II ($S = 1.018$, $W = 0.94$) and III ($S = 1.052$, $W = 0.81$) are displayed in Fig. 5. Positron lifetime measurements[19] show a annihilation fraction of $\eta = 0.34$ in the dominant positron trap for sample II. Based on this, the characteristic line-shape parameters for the dominant defect in sample II are estimated as 1.051 and 0.83 for S and W, respectively. This is close to the as-measured line-shape parameters of sample III. For this sample no lifetime data is available. In Fig. 6(b) the respective ratio curves recorded with coincidence Doppler measurements are displayed. The extrapolated ratio curve of both sample II and the as-measured spectrum of sample III show a very similar line shape. The bigger scatter in the former is due to a smaller annihilation fraction.

Compared to sample I, the as-grown samples II and III show several differences in their ratio curves. First, the intensity in the peak center region is clearly increased. The intensity difference to the InN lattice is thereby magnified by ∼35% compared to the spectrum of sample I. This is supported by very accurate statistics in this spectral region. Second, a significant decrease of the shoulder at 1.2 a.u. is visible, also with high statistical accuracy. Third, the drop at 2 a.u. is less pronounced, followed by slightly higher intensities in the high momentum region of the spectrum. Nevertheless, stronger scatter starts to dominate this region.

A comparison with the calculated defect spectra in Sec. III reveals that these changes coincide with the effects of the decoration of a V_{In} by V_N, as presented in Fig. 3(b). Especially the characteristic decrease of the shoulder at 1.2 a.u. in ratio curves of the experimental spectra cannot be correlated with any other calculated vacancy defect complex (see additionally Hautakangas *et al.*[24]). This is also expressed in the observed deviation of the characteristic line-shape parameters of samples II and III from the line determined by the characteristic points of sample I and the InN lattice in Fig. 5. A similar trend can be observed for the calculated V_{In}-nV_N parameters in Fig. 4. Judging from the amount of the observed changes in the ratio plots, an identification of the experimental spectra with V_{In}-V_N is most feasible, with possible influence from the V_{In}-$2V_N$. This assignment is in good agreement with the positron lifetime data.[19]

C. Defects at the interface

At higher implantation energies strong changes in the Doppler broadening signal are observed for samples I and II, and S (W) parameters of 1.039 (0.90) and 1.040 (0.90) are measured in samples I and II, respectively, in the region close to the interface with the buffer layer (see Fig. 5). From positron lifetime data in this region[7,19] we determine positron annihilation fractions of $\eta = 0.47$ and $\eta = 0.52$ at the dominant positron traps in samples I and II, respectively. The characteristic defect lifetime at the interface is slightly increased compared to the layer region. The extrapolated line-shape parameters are determined as 1.083 (0.78) and 1.077 (0.81) for S (W) in samples I and II, respectively, and show an even stronger deviation from the line defined by the characteristic points of sample I and the InN reference as already observed in Sec. IV B. The characteristic SW points of both interfaces coincide within the statistical accuracy. This indicates that the same dominant positron trap is present in both samples, which is also shown in the extrapolated ratio curves shown in Fig. 6(c). In both samples a strong increase in the peak center intensity to ∼1.12 is visible, which is over twofold compared to that observed in the irradiated layer. Additionally, the signal drops straight to the minimum at 2 a.u. without showing anymore the shoulder which is visible in the layer region of both samples. The observed trends are qualitatively very similar to the ones described in the previous section for the layer region of samples II and III, but are

intensified. Therefore, we identify the induced changes with an increase in the decoration of V_{In} with V_N. When comparing to the calculated momentum distributions in Sec. III, the best agreement is found for the spectrum of the V_{In}-3V_N complex. Results from both conventional Doppler broadening (Fig. 5) and positron lifetime spectroscopy additionally support this assignment.[19,38]

D. Summary and discussion

Based on the above-presented data we are able to identify the dominant positron trap created in high-energy particle irradiation of MBE-grown InN layers as the isolated V_{In}, while in as-grown MBE and MOCVD material the observed defect is a mixed V_{In}-V_N vacancy complex. The changes at the interface in both irradiated material and as-grown layers are assigned to the formation of larger V_{In}-nV_N complexes with an average of $\sim$3V_N surrounding the V_{In}. It has to be noted that the positron implantation profile for the chosen interface point (12 keV) is already considerably broadened and hence the signal from a wide area of the layer is averaged. The observed complexing of V_{In} and V_N is in good agreement[39] with existing data on the electron mobility in these samples[3] and might be the reason behind observed superior transport properties.

The measured Doppler broadening of the annihilation γ radiation is caused by the momentum component of annihilating e-p pairs along the detection direction.[14] All our experimental spectra are recorded perpendicular to the c axis but the exact detection direction in the c plane is not identified. We compare the experimental spectra to computational momentum distributions integrated over the m plane. The induced uncertainty could in principle cause difficulties for the exact defect identification, as small differences between the different lattice directions are present.[31] Nevertheless, these are minor compared to differences between the calculated spectra of different defect complexes and hence pose no problem in our case. This counts especially when interpreting changes in the momentum distributions rather than absolute values.

Our data accentuates the advantage of high-quality coincidence Doppler[26] spectra for the identification of defect identities. Apart from the advanced experimental resolution compared to conventional Doppler measurements which helps to distinguish defect-induced changes [see Fig. 3(a)], important features in the spectra might be lost when only regarding the integrated line-shape parameters S and W. This is the case, e.g., for the observed disappearance of the shoulder at 1.2 a.u., which is identified as a unique feature of the V_{In}-nV_N complexes. The commonly used integration windows for the S and W parameters cannot include this momentum area, in order to avoid correlation effects.[14] Irrespective of this, a shift of the lower limit of the W-parameter window to 2.2 a.u. (for a detector resolution of 1.24 keV) would be beneficial in future positron experiments in InN in order to maximize the visibility of defect-induced changes (see Fig. 3).

V. CONCLUSION

We present the identification of dominant vacancy-type positron traps in different representative InN samples by combining positron lifetime and Doppler broadening spectroscopy with *ab initio* calculations of the positron annihilation characteristics. Calculated momentum distributions of annihilating electron positron (e-p) pairs in different vacancy-type defects are compared to high-resolution measurements of the Doppler broadened e-p annihilation radiation acquired with the coincidence Doppler technique. We find that isolated V_N or pure V_N complexes do not trap positrons. During high-energy particle irradiation isolated V_{In} are created, which are the dominant positron traps in such samples at room temperature. In as-grown InN samples, on the other hand, V_{In} do not occur isolated but complexed with one or more V_N. The observed changes of the Doppler broadening signal close to the interface are identified with an increasing amount of V_N surrounding the V_{In}. The characteristic lifetimes, ratio curves, and S and W parameters for the identified defects are determined.

ACKNOWLEDGMENTS

The authors thank the groups of W. Schaff at Cornell University, J. Speck at University of California Santa Barbara, and O. Briot at Université Montpellier II for the generous supply of InN samples. F. Reurings is acknowledged for his help with positron lifetime measurements. This work has been supported by the European Commission under the 7th Framework Program through the Marie Curie Initial Training Network RAINBOW, Contract No. PITN-Ga-2008-213238.

*christian.rauch@tkk.fi

[1] P. D. C. King, T. D. Veal, P. H. Jefferson, S. A. Hatfield, L. F. J. Piper, C. F. McConville, F. Fuchs, J. Furthmüller, F. Bechstedt, H. Lu *et al.*, Phys. Rev. B **77**, 045316 (2008).

[2] A. G. Bhuiyan, A. Hashimoto, and A. Yamamoto, J. Appl. Phys. **94**, 2779 (2003).

[3] R. E. Jones, S. X. Li, E. E. Haller, H. C. M. van Genuchten, K. M. Yu, J. W. Ager III, Z. Liliental-Weber, W. Walukiewicz, H. Lu, and W. J. Schaff, Appl. Phys. Lett. **90**, 162103 (2007).

[4] S. X. Li, K. M. Yu, J. Wu, R. E. Jones, W. Walukiewicz, J. W. Ager, W. Shan, E. E. Haller, H. Lu, and W. J. Schaff, Phys. Rev. B **71**, 161201 (2005).

[5] L. F. J. Piper, T. D. Veal, C. F. McConville, H. Lu, and W. J. Schaff, Appl. Phys. Lett. **88**, 252109 (2006).

[6] F. Tuomisto, A. Pelli, K. M. Yu, W. Walukiewicz, and W. J. Schaff, Phys. Rev. B **75**, 193201 (2007).

[7] F. Reurings, C. Rauch, F. Tuomisto, R. E. Jones, K. M. Yu, W. Walukiewicz, and W. J. Schaff, Phys. Rev. B **82**, 153202 (2010).

[8] C. Stampfl, C. G. Van de Walle, D. Vogel, P. Krüger, and J. Pollmann, Phys. Rev. B **61**, R7846 (2000).

[9] X. M. Duan and C. Stampfl, Phys. Rev. B **77**, 115207 (2008).

[10] X. M. Duan and C. Stampfl, Phys. Rev. B **79**, 035207 (2009).

[11] X. M. Duan and C. Stampfl, Phys. Rev. B **79**, 174202 (2009).

[12] C. G. Van de Walle, J. L. Lyons, and A. Janotti, Phys. Status Solidi A **207**, 1024 (2010).

[13] I. Mahboob, T. D. Veal, C. F. McConville, H. Lu, and W. J. Schaff, Phys. Rev. Lett. **92**, 036804 (2004).

[14]K. Saarinen, P. Hautojärvi, and C. Corbel, *Positron Annihilation Spectroscopy of Defects in Semiconductors*, Semiconductors and Semimetals Vol. 51A (Academic, New York, 1998).
[15]J. Oila, A. Kemppinen, A. Laakso, K. Saarinen, W. Egger, L. Liszkay, P. Sperr, H. Lu, and W. J. Schaff, Appl. Phys. Lett. **84**, 1486 (2004).
[16]A. Laakso, J. Oila, A. Kemppinen, K. Saarinen, W. Egger, L. Liszkay, P. Sperr, H. Lu, and W. J. Schaff, J. Cryst. Growth **269**, 41 (2004).
[17]F. Reurings, F. Tuomisto, C. S. Gallinat, G. Koblmüller, and J. S. Speck, Appl. Phys. Lett. **97**, 251907 (2010).
[18]A. Pelli, K. Saarinen, F. Tuomisto, S. Ruffenach, and O. Briot, Appl. Phys. Lett. **89**, 011911 (2006).
[19]C. Rauch, F. Reurings, F. Tuomisto, T. D. Veal, C. F. McConville, H. Lu, W. J. Schaff, C. S. Gallinat, G. Koblmüller, J. S. Speck *et al.*, Phys. Status Solidi A **207**, 1083 (2010).
[20]H. Wang, D. S. Jiang, L. L. Wang, X. Sun, W. B. Liu, D. G. Zhao, J. J. Zhu, Z. S. Liu, Y. T. Wang, S. M. Zhang *et al.*, J. Phys. D **41**, 135403 (2008).
[21]W. Walukiewicz, Physica B **302-303**, 123 (2001).
[22]A. Uedono, S. F. Chichibu, M. Higashiwaki, T. Matsui, T. Ohdaira, and R. Suzuki, J. Appl. Phys. **97**, 043514 (2005).
[23]A. Uedono, S. Ishibashi, T. Ohdaira, and R. Suzuki, J. Cryst. Growth **311**, 3075 (2009).
[24]S. Hautakangas, I. Makkonen, V. Ranki, M. J. Puska, K. Saarinen, X. Xu, and D. C. Look, Phys. Rev. B **73**, 193301 (2006).
[25]I. Makkonen, M. Hakala, and M. J. Puska, Phys. Rev. B **73**, 035103 (2006).
[26]K. G. Lynn, J. R. MacDonald, R. A. Boie, L. C. Feldman, J. D. Gabbe, M. F. Robbins, E. Bonderup, and J. Golovchenko, Phys. Rev. Lett. **38**, 241 (1977).
[27]M. Alatalo, B. Barbiellini, M. Hakala, H. Kauppinen, T. Korhonen, M. J. Puska, K. Saarinen, P. Hautojärvi, and R. M. Nieminen, Phys. Rev. B **54**, 2397 (1996).
[28]E. Boroński and R. M. Nieminen, Phys. Rev. B **34**, 3820 (1986).
[29]P. E. Blöchl, Phys. Rev. B **50**, 17953 (1994).
[30]G. Kresse and J. Furthmüller, Phys. Rev. B **54**, 11169 (1996).
[31]C. Rauch, I. Makkonen, and F. Tuomisto, Phys. Status Solidi A **208**, 1548 (2011).
[32]*Properties of Group-III Nitrides*, edited by J. H. Edgar, EMIS Datareviews Series No. 11 (IEE, London, 1994).
[33]M. J. Puska and R. M. Nieminen, J. Phys. F **13**, 333 (1983).
[34]F. Tuomisto, K. Saarinen, T. Paskova, B. Monemar, M. Bockowski, and T. Suski, J. Appl. Phys. **99**, 066105 (2006).
[35]J. Neugebauer and C. G. V. de Walle, Appl. Phys. Lett. **69**, 503 (1996).
[36]W. J. Schaff, H. Lu, L. F. Eastman, W. Walukiewicz, K. M. Yu, S. Keller, S. Kurtz, B. Keyes, and L. Gevilas, in *State-of-the-Art Program on Compound Semiconductors XLI and Nitride and Wide Bandgap Semiconductors for Sensors, Photonics, and Electronics V*, edited by H. M. Ng and A. G. Baca, The Electrochemical Society Proceedings Series Vol. 2004-06 (Electrochemical Society, Honolulu, HI, 2004), p. 358.
[37]B. Maleyre, O. Briot, and S. Ruffenach, J. Cryst. Growth **269**, 15 (2004).
[38]F. Reurings, F. Tuomisto, W. Egger, B. Loewe, L. Ravelli, S. Sojak, Z. Liliental-Weber, R. E. Jones, K. M. Yu, W. Walukiewicz *et al.*, Phys. Status Solidi A **207**, 1087 (2010).
[39]C. Rauch, I. Makkonen, F. Tuomisto, P. D. C. King, T. D. Veal, and C. F. McConville (unpublished).